

# Numerical Study about the Influence of Small Casting Speed Variations on the Metallurgical Length in Continuous Casting of Steel Slabs

Josef Domitner,\* Menghuai Wu, and Andreas Ludwig

Numerical simulations are prepared to investigate the influence of small casting speed variations between 715 and 735 mm min<sup>-1</sup> on the metallurgical length in continuous casting of 285 mm thick steel slabs. The effect of considering/ignoring the melt flow in the numerical continuous casting model for predicting the metallurgical length is also investigated. The simulations are based on an Eulerian two-phase solidification model including melt (liquid phase) and columnar dendrites (solid phase). Solidification of a binary Fe-C-alloy is calculated. Two 25 m long straight strand geometries of industrial scale are modeled. Both of these geometries have waved surfaces to consider periodical strand surface bulging. In order to consider a defined mechanical softreduction (MSR) configuration as well, the cross-section of one of these geometries decreases at a rate of 1 mm m<sup>-1</sup> within a defined length. For a given casting configuration and for defined cooling conditions, the influence of small casting speed variations on the metallurgical length, on the average solid fraction and on the enthalpy flux are determined. The simulation results can be used to optimize the settings for operating continuous casting plants, e.g., to adapt the MSR position.

## 1. Introduction

The length of the liquid core inside of continuously cast strands is an important parameter for characterizing and controlling the casting process. For example, the positions of mechanical softreduction (MSR) segments or electromagnetic stirring devices are adapted to the centerline solid fraction of the cast strand, which is influenced by this so-called “metallurgical length”.<sup>[1–3]</sup> In order to calculate the thickness of the solidifying strand shell and therefore to estimate the metallurgical length, mathematical solidification modeling became increasingly important during the last decades. A comprehensive overview about this field of research is provided by Thomas.<sup>[4]</sup> Thanks to the availability of sufficient computational power complex industrial plant conditions can be modeled nowadays. For example, employing numerical models for real-time and in-line strand cooling optimization is of common practice in the steel production industry.<sup>[5–11]</sup> However, most

numerical continuous casting models are simply based on heat transfer calculations. It is important to note that these thermal or thermo-mechanical models do not consider the influence of different melt flow phenomena on the evolving solidification front. Particularly in the mould region of a continuous caster the flow may distinctly influence the initial strand shell formation.<sup>[12]</sup> Furthermore, the formation of macrosegregation and the microstructure evolution inside the strand are affected by relative motion between the liquid and the solid.<sup>[13]</sup> Therefore, several authors consider melt flow in their numerical continuous casting models.<sup>[14–20]</sup> In the current work, the flow caused by shrinkage feeding and by strand shell deformation due to surface bulging and MSR is covered with the numerical model applied to determine the metallurgical length. An additional simulation case ignoring the feeding flow phenomenon is also prepared for comparison, and the influence of constant and varying solid phase velocities inside the MSR zone on the metallurgical length is investigated.

---

[\*] J. Domitner, M. Wu, A. Ludwig  
Chair of Simulation and Modeling of Metallurgical Processes, University of Leoben, Leoben, Austria  
Email: josef.domitner@unileoben.ac.at  
M. Wu  
Christian Doppler Laboratory for Advanced Process Simulation of Solidification and Melting, University of Leoben, Leoben, Austria

## 2. Numerical Model

1. Two slightly different geometries of a 25 m long and 285 mm thick cast strand are investigated: geometry G1, which ignores and geometry G2, which considers

DOI: 10.1002/srin.201400059

MSR. Within the MSR zone the cross-section of the strand is reduced at a rate of  $1 \text{ mm m}^{-1}$ . Each of these model geometries is meshed with a regular 2D mesh, which has an approximate element size of  $5 \text{ mm} \times 5 \text{ mm}$ .

2. Solidification of the cast strand is calculated with an Eulerian two-phase model. It is a simplified version of the three-phase volume-averaging solidification model developed by Wu and Ludwig,<sup>[21–23]</sup> which is based on the work of Beckermann and co-authors.<sup>[24,25]</sup>
3. Two phases are considered: the melt (“liquid”) and the columnar dendrites (“solid”). For both phases, the conservation equations of mass, species, and enthalpy are solved. However, the momentum equation is only solved for the liquid, because the motion of the solid is predefined analytically.
4. The complex morphology of the columnar dendrites is simplified with cylinders of constant spacing and regularly staggered alignment. Interdendritic melt flow is caused by solidification shrinkage and by strand surface deformation due to bulging and MSR.
5. The solidification rate (mass transfer rate) is governed by diffusion in the liquid phase due to the different species concentrations at the cylindrical solid–liquid interface and of the surrounding melt. Back diffusion in the solid phase is neglected.
6. To ensure numerical stability of the simulations, the densities of the liquid and of the solid are assumed as equal beyond the solid fraction of 0.95. Hence, no relative motion between the dendrites and the melt and therefore no shrinkage feeding flow occurs beyond this limit.
7. Since thermo-mechanics are not considered, the movement of the solid phase is predefined analytically. Perpendicular to the casting direction the movement is related on the periodical bulging of the strand shell. When the solidification front reaches the strand centerline the mushy zone is compressed, which is expressed by decreasing the solid velocity exponentially.
8. In principle, the solid phase movement in casting direction is assumed to be equal to the constant casting speed (simulation cases G1, G2-I). However, according to the decreasing cross-section within the MSR zone a linearly increasing solid phase velocity component in casting direction is also considered (simulation case G2-II).
9. Since the influences of strand bending and gravity are neglected in the current model, a symmetry boundary condition at the totally straight strand center is applied. That halves the number of mesh elements and reduces the required calculation time. The periodically bulged strand surface is approximated with a sinusoidal contour of linearly decreasing amplitude.
10. The heat transfer (and therefore the cooling intensity) within the secondary cooling zone at the strand

surface is assumed as independent from the casting speed. This assumption is only valid when the casting speed variations are quite small. However, the heat transfer coefficient is defined as a function of the strand length coordinate to consider different cooling intensities at different sections of the secondary cooling zone.

**Table 1** provides an overview about the mechanisms modeled in the three simulation cases G1, G2-I, and G2-II. The model geometries and the meshes were generated with the pre-processing tool GAMBIT. The commercial software package FLUENT was then used to assign boundary conditions and material data and to perform the simulations. More detailed information about the numerical model is given at Domitner et al.<sup>[20]</sup>

### 3. Results

The solid fraction patterns obtained for simulation cases G1, G2-I, and G2-II are comparable in most regions of the cast strand. However, they differ considerably at the tip of the solidification crater, as illustrated in **Figure 1**. The solid fraction profiles are similar for simulation cases G1 (**Figure 1a**) and G2-II (**Figure 1c**). In both cases, the solid velocity  $v_{s,x}$  parallel to the casting direction is related to the cross-section of the strand.  $v_{s,x}$  is constant in case G1, but it increases linearly according to the cross-section reduction within the MSR zone in case G2-II. The solid fraction pattern of case G2-I (**Figure 1b**) looks different. There, the mushy zone is sharply notched at high solid fractions between  $f_s = 0.90$  and  $f_s = 0.95$ , resulting in a distinct peak at the strand center, which is accompanied by a protuberant “nose” beside. That indicates the blocking of the solid in casting direction due to the narrow cross-section behind the MSR zone. In the current study, the metallurgical length  $L$  is defined as the distance from the fully liquid melt pool level to the intersection between the isoline of  $f_s = 0.95$  and the strand centerline. Therefore, this length can be measured directly at the straight centerline of the modeled continuous casting strand. According to this definition,  $L$  becomes longer for simulation cases G1 and G2-II if the casting speed  $v^{\text{cast}}$  increases. However, for case G2-I the position of the intersection between the isoline of  $f_s = 0.95$  and the strand centerline does not change although  $v^{\text{cast}}$  increases.

| Simulation case   | G1 | G2-I | G2-II |
|---|----|------|-------|
| Mechanical softreduction (MSR)                              | No | Yes  | Yes   |
| Varying solid phase velocity $v_{s,x}$ in casting direction | No | No   | Yes   |

**Table 1.** Mechanisms modeled in the three simulation cases.

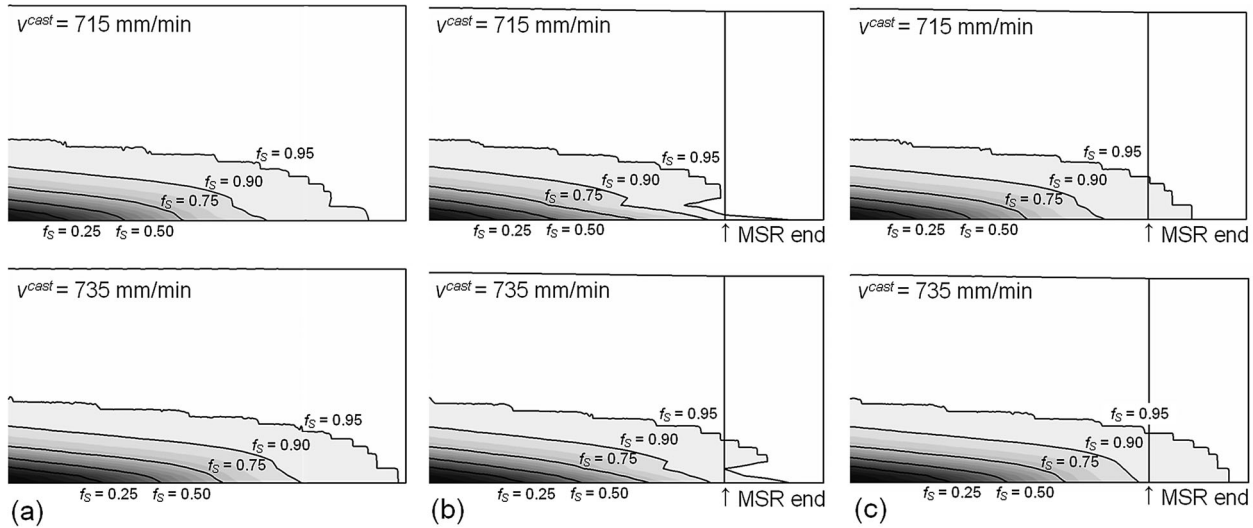


**Figure 1.** Comparison of the solid fraction patterns at the area of final solidification for simulation cases G1 (a), G2-I (b), and G2-II (c). Top row:  $v^{cast} = 715 \text{ mm min}^{-1}$ , bottom row:  $v^{cast} = 735 \text{ mm min}^{-1}$ . For proper visualization, the strand length is scaled by a factor of 1:25.

The general dependence of the metallurgical length  $L$  on the actual casting velocity  $v^{cast}$  is illustrated in **Figure 2**. Therein, the ascending lines indicate that  $L$  increases proportional to  $v^{cast}$  for cases G1 and G2-II, but the almost horizontal line implies that  $L$  is independent on the actual casting speed for case G2-I. However, the shape of the solidification crater changes although the metallurgical length does not increase, as shown in **Figure 1b**. To consider this phenomenon as well, the enthalpy flux ratio  $r_H$  is introduced, which is defined as

$$r_H = \frac{\dot{H}^{in} - \dot{H}^{out}}{\dot{H}^{in}} \quad (1)$$

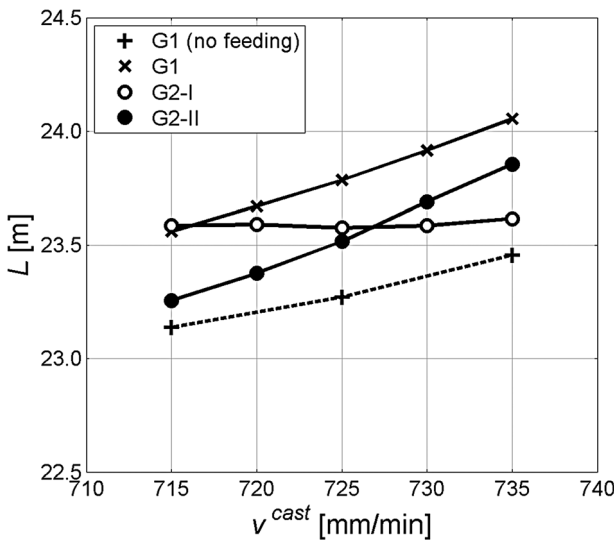


**Figure 2.** Metallurgical length  $L$  versus casting velocity  $v^{cast}$ . As shown exemplarily for simulation case G1,  $L$  is underestimated if shrinkage feeding flow is not considered.

$r_H$  quantifies the heat being extracted by strand surface cooling, which is equal to the reduction of the thermal energy within the cast length. From a practical point of view,  $r_H$  provides information about enhancing the strand cooling intensity to keep the metallurgical length constant if the process is operated with higher casting speed. Considering steady state conditions, the enthalpy fluxes  $\dot{H}^{in}$  at the inlet and  $\dot{H}^{out}$  at the outlet of the simulation domain are calculated with Equations 2 and 3. The strand cross-section is fully liquid at the inlet. Since solidification ends at  $f_s = 0.95$  in the current simulation model, the cross-section contains remaining liquid at the outlet, which must be taken into account for calculating  $\dot{H}^{out}$ .

$$\dot{H}^{in} = \dot{m}_L^{in}(\Delta H_m + c_{p,L} \bar{T}^{in}) \quad (2)$$

$$\dot{H}^{out} = \dot{m}_L^{out}(\Delta H_m + c_{p,L} \bar{T}^{out}) + \dot{m}_S^{out} c_{p,S} \bar{T}^{out} \quad (3)$$

$\dot{m}_L$  and  $\dot{m}_S$  are the mass flow rates of the liquid and of the solid.  $\bar{T}$  represents the average temperature at the inlet (superscript “in”) or at the outlet (superscript “out”) of the simulation domain, respectively.  $c_{p,L}$  and  $c_{p,S}$  are the specific heat capacities of the liquid and of the solid, which are assumed as equal in the current model. The latent heat of the melt,  $\Delta H_m$ , is released during solidification. Notice that Equation 4 must be valid to fulfil mass conservation.

$$\dot{m}_L^{in} = \dot{m}_L^{out} + \dot{m}_S^{out} \quad (4)$$

As illustrated in **Figure 3**, the enthalpy flux ratio  $r_H$  decreases linearly with increasing casting speed  $v^{cast}$ .  $r_H$  is directly proportional to  $\bar{f}_S$ , the average solid fraction of the cast strand. If  $v^{cast}$  increases, less time is available to extract the internal heat at a given strand length. Hence, less melt solidifies and therefore  $\bar{f}_S$  decreases. Accordingly,

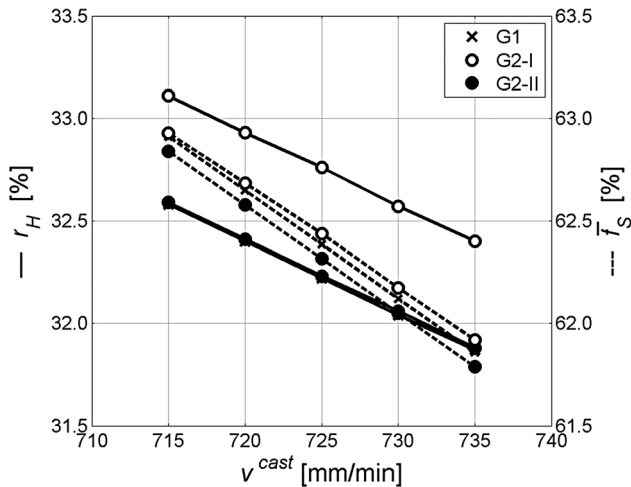


**Figure 3.** Enthalpy flux ratio  $r_H$  (continuous lines) and average solid fraction  $\bar{f}_S$  (broken lines) versus casting velocity  $v^{\text{cast}}$ . The lines representing  $r_H$  for cases G1 and G2-II overlap.

the solidification crater must widen up particularly beside the centerline of the strand in simulation case G2-I, because there the metallurgical length measured directly at the centerline is constant.

#### 4. Conclusions

In the present study, the influence of the casting velocity on the metallurgical length in continuous casting of steel slabs is investigated. Based on the performed simulations, the following conclusions are drawn:

1. Generally, the metallurgical length  $L$  increases proportionally to the casting speed  $v^{\text{cast}}$ . Increasing  $v^{\text{cast}}$  by  $10 \text{ mm min}^{-1}$  elongates  $L$  by  $0.25\text{--}0.30 \text{ m}$  for both casting configurations, with and without MSR. The small change in the metallurgical length in comparison to the strand length of  $25 \text{ m}$  is reasonable, because the variation of the casting speed is also quite small.
2. However, if the solid velocity in casting direction is treated as constant within the MSR zone, the increase of  $L$  cannot be observed directly at the strand centerline. For this case, the length difference is apparent at a certain distance apart from the center.
3. For a certain casting configuration including constant operating parameters and defined strand dimensions, the relationship between  $L$  and  $v^{\text{cast}}$  can be described by a linear approximation. Accordingly, estimating  $L$  for different casting speeds is possible, if  $L$  is known for a certain casting speed at least. This is helpful for adapting the MSR position.
4. The reduction in thermal energy is inverse proportional to  $v^{\text{cast}}$ , which is indicated by the decreasing enthalpy flux ratio  $r_H$ . Increasing  $v^{\text{cast}}$  by  $10 \text{ mm min}^{-1}$  decreases

$r_H$  by  $\approx 0.4\%$ . More intensive strand surface cooling would be a possibility to keep  $r_H$  and  $L$  constant even if  $v^{\text{cast}}$  increases.

5. If the melt flow which compensates the solidification induced volume shrinkage is not considered,  $L$  is underestimated by about  $0.5\text{--}0.6 \text{ m}$ .
6. Other process parameters besides the casting velocity (e.g., casting temperature, alloy composition, dimensions of the strand, cooling conditions) may influence the metallurgical length distinctly. To investigate the influence of these parameters is an ongoing work.

#### Acknowledgments

The authors would like to thank the Christian Doppler Research Association (CDG) as well as the industrial partners voestalpine Stahl GmbH, voestalpine Stahl Donawitz GmbH & Co KG and Siemens VAI Metals Technologies GmbH & Co for the financial support of this work.

Received: February 22, 2014

**Keywords:** steel; continuous casting; metallurgical length; multiphase simulation

#### References

- [1] A. Reichert, K.-H. Tacke, K. Harste, M. Hecht, J. Heilemann, U. Ölmann, K. Schwerdtfeger, B. Barber, R. C. Beaverstock, R. Walmsley, *Casting and Solidification – Strand Reduction in Continuous Casting and Its Effect on Product Quality*, European Commission, Luxembourg 2002.
- [2] R. Thome, K. Harste, *ISIJ Int.* **2006**, *46*, 1839.
- [3] S. Luo, M. Y. Zhu, C. Ji, Y. Chen, *Ironmaking Steelmaking* **2010**, *37*, 140.
- [4] B. G. Thomas, *Metall. Mater. Trans. B* **2002**, *33B*, 795.
- [5] S. Barozzi, P. Fontana, P. Pragliola, *Iron Steel Eng.* **1986**, *62*, 21.
- [6] K. Okuno, H. Naruwa, T. Kuribayashi, T. Takamoto, *Iron Steel Eng.* **1987**, *63*, 34.
- [7] K.-H. Spitzer, K. Harste, B. Weber, P. Monheim, K. Schwerdtfeger, *ISIJ Int.* **1992**, *32*, 848.
- [8] S. Louhenkilpi, E. Laitinen, R. Nieminen, *Metall. Trans. B* **1993**, *24B*, 685.
- [9] K. Mörwald, K. Dittenberger, K. D. Ives, *Ironmaking Steelmaking* **1998**, *25*, 323.
- [10] R. A. Hardin, K. Liu, A. Kapoor, C. Beckermann, *Metall. Mater. Trans. B* **2003**, *34B*, 297.
- [11] B. Petrus, K. Zheng, X. Zhou, B. G. Thomas, J. Bentsman, R. O'Malley, *Metall. Mater. Trans. B* **2011**, *42B*, 87.

- [12] B. G. Thomas, L. Zhang, *ISIJ Int.* **2001**, *41*, 1181.
- [13] G. Lesoult, *Mater. Sci. Eng. A* **2005**, *413–414*, 19.
- [14] P. J. Flint, in: *Proc. of 73rd Steelmaking Conf.*, Iron and Steel Society of AIME, Warrendale, PA **1990**, p. 481.
- [15] B. G. Thomas, L. J. Mika, F. M. Najjar, *Metall. Mater. Trans. B* **1990**, *21B*, 387.
- [16] M. R. Aboutalebi, M. Hasan, R. I. L. Guthrie, *Metall. Mater. Trans. B* **1995**, *26B*, 731.
- [17] S. K. Choudhary, D. Mazumdar, *Steel Res.* **1995**, *66*, 199.
- [18] F. Mayer, M. Wu, A. Ludwig, *Steel Res. Int.* **2010**, *81*, 660.
- [19] M. Wu, J. Domitner, A. Ludwig, *Metall. Mater. Trans. A* **2012**, *43A*, 945.
- [20] J. Domitner, M. Wu, A. Kharicha, A. Ludwig, B. Kaufmann, J. Reiter, T. Schaden, *Metall. Mater. Trans. A* **2014**, *45A*, 1415.
- [21] A. Ludwig, M. Wu, *Mater. Sci. Eng. A* **2005**, *413–414*, 109.
- [22] M. Wu, A. Ludwig, *Metall. Mater. Trans. A* **2006**, *37A*, 1613.
- [23] M. Wu, A. Ludwig, *Metall. Mater. Trans. A* **2007**, *38A*, 1465.
- [24] J. Ni, C. Beckermann, *Metall. Trans. B* **1991**, *22B*, 349.
- [25] C. Beckermann, R. Viskanta, *Appl. Mech. Rev.* **1993**, *46*, 1.